IEEE Access
Multidisciplinary | Rapid Review | Open Access Journal

Received November 18, 2019, accepted December 3, 2019, date of publication December 10, 2019,
date of current version December 23, 2019.

Digital Object Identifier 10.1109/ACCESS.2019.2958650

An Improved Sensorless Control Strategy of Ship IPMSM at Full Speed Range

ZHENRUI ZHANG[1], HAOHAO GUO[1], YANCHENG LIU[1], QIAOFEN ZHANG[2], PENGLI ZHU[1], AND RASHID IQBAL[1]

[1]Marine Engineering Department, Dalian Maritime University, Dalian 116026, China
[2]Marine Electrical Engineering Department, Dalian Maritime University, Dalian 116026, China

Corresponding author: Yancheng Liu (liuyc3@126.com)

This work was supported in part by the National Natural Science Foundation of China under Grant 51979021, Grant 51479018, and Grant 51709028, in part by the Fundamental Research Funds for the Central Universities under Grant 3132019317, and in part by the Liaoning Provincial Key Research and Development Program under Grant 2017220005.

ABSTRACT This paper proposed an improved sensorless control strategy for ship electric propulsion which bases on I/f control and back electromotive force integral (EMF), suppressing the speed fluctuation during algorithm switching, improving the flux estimation accuracy of internal permanent magnet synchronous motors (IPMSMs) and achieving the stable operation of the motor. Firstly, this strategy was adopted for controlling the stator current during the switching process to improve speed fluctuation. Then, a simple flux estimation method is presented by rewriting the mathematical model of IPMSM. To achieve the result which overcomes the problem of flux estimation and current measurement errors and improved LPF was developed which solved the phase delay and DC-offset problem of flux estimation. Finally, the propeller load platform is under construction to verify the effectiveness of the control strategy. Experimental results show that the system based on this method works smoothly and it has better speed tracking performance.

INDEX TERMS I/f control, IPMSM, switching strategy, back EMF, sensorless control algorithm.

I. INTRODUCTION

In past few years, due to reduction of the cost of permanent magnetic materials and the development of high performance processors, PMSMs are widely applied in the industry because of the many advantages such as high efficiency, high power density, and fast dynamic response. [1]–[3]. Meanwhile, with the world's attention to environmental protection and the continuous development of ship electric propulsion, lots of vessels are powered by PMSMs [4]–[9]. The acquisition of rotor position information is critical to the control performance in the PMSM vector control systems or direct torque control systems. Therefore, the encoder is required to obtain rotor position information. However, the high-precision position sensor is expensive and the ship's propulsion motor is worked in harsh environments such as severe pressure, humidity and vibration. Under these conditions, the traditional mechanical encoder will not work normally [10]. Therefore, the sensorless control algorithm has received extensive attention, and rapid development [11]. At present, it is mainly divided into two categories: one is the high-frequency injection method [12], which can be divided into three categories again: rotary signal injection method [13], the pulse signal injection method [14] and square signal injection method [15], and these methods are applied at zero and low speed. So, it has certain limitations and requires higher hardware controllers. The other type is the back EMF control algorithm [16]. This method has several types such as Luenberger observer [17], flux observer [18], [19], sliding mode observer [20], model reference adaptive [21] and so on. When the motor speed is low, the value of back EMF is so small that the signal to noise ratio is poor. So due to this reason, back EMF algorithm can only be applied to high speed, and proper methods are needed to start the motor from zero speed.

Some scholars have proposed the V/f control algorithm to start the motor at zero speed [22]. As no closed-loop control, this method loses synchronization and even fails to start when there is a heavy load. The I/f control algorithm with current closed-loop compensates this deficiency of the V/f control algorithm. At the same time, it also can achieve maximum output torque at the starting time, which can be

The associate editor coordinating the review of this manuscript and approving it for publication was Zhuang Xu.

implemented to fans, pumps, compressors, propellers, and other load occasions. But this algorithm lowers the efficiency of the driving system. It is, therefore, necessary to adopt a more efficient back EMF algorithm when machine startup and reach a medium or high speed [23]. If the two algorithms directly switch, the speed and torque will fluctuate. Therefore, it is necessary to control the stator current during the switching process. Paper mentioned the first-order lag compensator scheme [24]. This method is only applicable for the rotor angle, but the current fluctuation at the moment of switching is very large, which produced a great fluctuation in the shafting. Error angle at the switching time is taken into account in paper [25], but the rate of change of current during the switching process is not considered. Due to this, it affects the fluctuation of rotational speed. A fixed-slope stator current control method proposed in the article [26], which is simple and easy to implement, but the speed and current fluctuation are still obvious. To decrease the influence of switching algorithm on system stability, a new switching method considering both the position of the switching point and the change in the current rate in the process is proposed in this paper.

Back EMF is a fundamental and reliable speed estimation algorithm in the medium and high-speed control algorithm. The motor voltage integral model is utilized to calculate the flux linkage and rotor position. However, there are certain shortcomings in back EMF itself. First, the initial value of the integrator will cause the flux offset obtained by integration. Second, when sampling contains DC offset, the integral operation in the program will lead to zero drift, which will lead to the incorrect result of the flux. In [27], LPF is applied to calculate flux and avoid the problem from integral operations. However, LPF can only suppress but not solve the offset problem in sampling current. At the same time, LPF will also lead to a flux phase delay. This paper introduced an improved control strategy for the above mention problems. Third, the control algorithms in different types of PMSMs are inconsistent. The mathematical model of the IPMSMs is complex compared with the surface-mounted permanent magnet (SPMSM). So, a state observer is needed to observe rotor flux linkage [28]. To solve this problem, a method for estimating the rotor position of the salient pole motor based on extended back EMF method is given in [29]. Although this method is efficient, calculating involves much work, and an angle observer is required. In [30], the concept of active flux is proposed. Based on this paper, [31] derived a new method to estimate the rotor position using only the q-axis inductance, which is helpful to reduce the complexity of the algorithm for estimating the flux of IPMSM, but this scheme is not useful to solve the integral initial value and zero drift problem introduced by the back EMF algorithm.

This paper presented the switching problem of IPMSM motor from I/f control to double closed-loop control and the defects of the back EMF integration algorithm. The stator current control strategy is explained in this article which improves the system stability of the switching process.

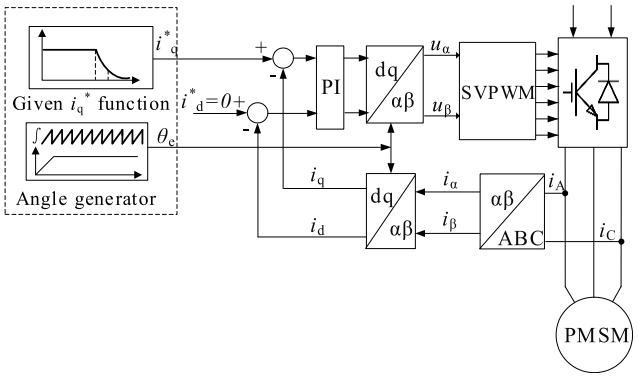

FIGURE 1. Control structure diagram of I/f control of PMSM.

Then this strategy proposed an improved back EMF algorithm to analyze the mathematical model of the motor. The improved LPF which can eliminate DC offset error completely is used to find flux instead of the integral operation, which ensures accuracy of estimated rotor position. Finally, the sensorless control strategy was tested using simulation and experimental setup. This scheme has implemented in the marine propulsion motor of the laboratory with propeller load [32], [33]. Simulation and experimental results were discussed and presented in this paper.

II. I/F CONTROL AND SWITCHING STRATEGY FOR PMSM

I/f control consists of current closed-loop and speed open-loop control algorithm, which is generally applicable to the starting process of PMSM. As shown in Fig. 1, the electrical angle (θ_e) is calculated by angle generator integrating scheme is used to find electrical angular velocity ω_e rather than by encoder. θ_e participates in the park transformation and inverse park transformation in vector control scheme. Meanwhile setting the current-function controls the q-axis current i_q^* in place of the speed loop, which constitutes the vector control system of the speed open-loop and current closed-loop.

The I/f control mainly consists of three processes: the rotor pre-positioning process which initializes the rotor position of the motor; the constant current acceleration process which makes the motor speed reach the back EMF algorithm's requirement; the smooth switching process from the I/f to back EMF algorithm. The following paper discusses these processes.

A. I/F STARTUP PROCESS FOR PMSM

When the motor is stationary, the real rotor d-q reference frame is set to advance the synchronous rotating d*-q* reference frame by $\theta_L = 90°$ [34] and θ_L is the angle between the real rotor d-q reference frame and the synchronous rotating d*-q* reference frame. As shown in Fig.2(a), the d*-q* reference frame follows ω_e rotation. Fig.2(b) showed that electro-magnetic torque $T_e = K_T i_q^* \cdot \cos\theta_L$($K_T$ is the torque constant) is balanced with the starting torque T_{L0}, so that the motor can provide enough torque for starting. In this paper,

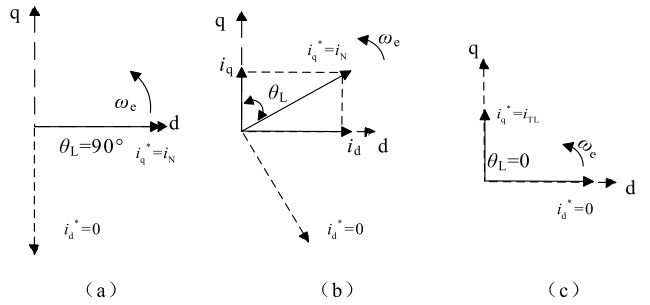

FIGURE 2. Phase diagram of d-q reference frame and d*-q* reference frame in I/f control: (a) Motor stationary moment (b) During acceleration of rotor (c) When $i_q^* = i_{TL}$(i_{TL} is the q-axis current balanced with the load).

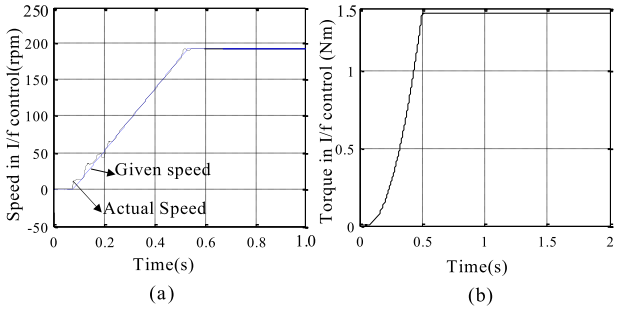

FIGURE 3. Simulation results of the motor starting process: (a) 0-0.5s Motor speed (b) 0-2s Motor given torque.

i_q^* is set to the rated current value i_N. With θ_L decreases, until T_e is greater than T_{L0}, the d-q reference frame rotates following the d*-q* reference frame, and the motor starts successfully. Therefore, the method of pre-positioning should be utilized to ensure the successful start of the motor, but the rotor may stay at positioning the dead zone in the process of pre-positioning, and the positioning failure can be avoided by using the orthogonal complement positioning method twice.

The primary purpose of the I/f control is to increase the motor speed from zero to the requirement of speed in back EMF. After the motor starts smoothly, the value of i_q^* is the rated value i_N, and the acceleration at a given speed is constant. The following paper will give the basis for designing the acceleration of the process.

According to the torque characteristics of the wind turbine load, the literature [26] gives a design methodology of speed acceleration by analyzing the mathematical model of the motor torque during the acceleration process. The angular velocity ω_e can be expressed as:

$$\omega_e = K_\omega t \tag{1}$$

where K_ω is the slope coefficient of speed which controls the acceleration of speed and it takes a fixed value in this paper. t is the time.

In this process of constant acceleration, the final stable rotational speed can be determined by the average torque $T_{e,ave}$, so that K_ω can be expressed as:

$$T_{e,ave} = K_T i_q^* \cos\theta_{L,ave} \tag{2}$$

$$K_\omega = p\frac{K_T i_q^* \cos\theta_{L,ave} - T_{L,ave}}{J} \tag{3}$$

where p and J is pole pairs and inertia; $\theta_{L,ave}$, and $T_{L,ave}$ is the θ_L and load torque average value in the 0-t time. The propeller load characteristics are similar to fan type load, and the magnitude of the torque is related to the motor speed. In this paper, the $T_{L,ave}$ of this process can be calculated by propeller load, but the value of $\theta_{L,ave}$ is challenging to estimate. Consider a limit case, as shown in Fig. 2(c), when $\theta_L = 0$, the maximum acceleration of speed can be obtained, and K_ω is limited to the range of the following formula:

$$K_\omega < p\frac{K_T i_q^* - T_{L,max}}{J} \tag{4}$$

where $T_{L,max}$ is the maximum load torque during startup. It can be seen from equation (3) that in the motor starting process, i_q^* cannot exceed the rated current of the motor, if J or T_L is large, the acceleration should be designed to be smaller.

A simulation was carried out to verify the feasibility of the above method. The propeller load was used during the experiment. The steady speed was set at 190 rpm, which is around a quarter of the rated speed. Experimental results show that the smaller the acceleration slope K_ω, the smaller the speed fluctuation. Considering the stability and rapidity of the system, the acceleration of 6 r/s^2 can meet the requirements. Fig.3(a) demonstrates that the motor's starting process when the acceleration is set to 6 r/s^2. Fig. 3(b) shows the load curve of propeller load characteristics, which is related to speed [7].

B. CONTROL METHOD DURING SWITCHING

As noted above, the value of i_q^* is set in as large as possible to make the motor have good starting performance. However, as shown in Fig. 2(b), i_q^* is larger than i_q, and the phase always lags behind i_q. Error angle θ_L causes that the motor d-axis current component is not zero. When the rotor flux increases, the motor is prone to magnetic saturation, which affects the motor parameters and causes the motor to run unstable. Therefore, it is necessary to shorten the time of the process.

In order to obtain better control performance and reduce the influence of I/f control on the motor parameters, after the rotor speed reaches the set speed, it needs to switch to the double closed-loop control strategy based on back EMF. Currently, T_e is constant. The value of θ_L is going to get smaller as i_q^* gets smaller. So, designing a suitable deceleration slope K_c is the key to the switching process. The design of this parameter will be analyzed below.

When the load torque is constant, according to Fig. 2(b), the relationship between i_q^* and θ_L satisfies the following formula:

$$i_q = i_q^* \cos\theta_L \tag{5}$$

Reference [26] uses a method of reducing i_q^* with a fixed slope. And put it into equation (5), we can get the graph of the change of θ_L with i_q^*.

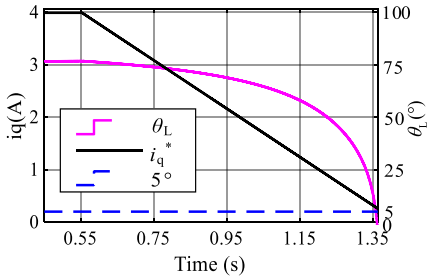

FIGURE 4. The error angle θ_L follows the curve of the given q-axis current i_q^*.

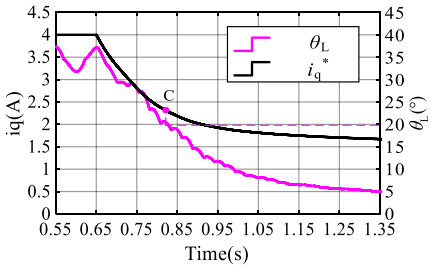

FIGURE 5. The error angle θ_L follows the i_q^* curve controlled by the method of this paper.

From Fig. 4, i_q^* is reduced from 4A to 0.2A, and θ_L is reduced from 75° to 0°. In this period, the change rate of i_q^* is fixed, but the rate of change of θ_L is faster and faster. The closer the i_q^* is to the i_q, the greater the rate at which θ_L converges to zero. I/f switching is performed in the way of [25], θ_L changes slowly with the decrease of i_q^* at the initial stage of switching, but θ_L decreases rapidly when i_q^* decreases in the later stage of switching. If switching at this condition, it will cause i_q and speed fluctuation inevitable. Therefore, the decreasing rate of θ_L needs to be decreased in the later period.

In this paper, θ_L is used as the slope coefficient, and a novel method for reducing the slope of q-axis current is proposed. The system automatically adjusts the slope rate. In this method, the law of the given current i_q^* value changing with time can be expressed by the following formula:

$$i_q^*(t) = i_{q0}^* - K_c \cdot \theta_L^2 \tag{6}$$

In the formula, i_{q0}^* is the maximum current value at the initial time, and K_c is the slope coefficient of current which controls the acceleration of current and it takes different values at different error angles scope.

In this paper, it is divided into two segments according to the value of θ_L. As can be seen from Fig. 5, in the process of controlling the current, a switching point C is designed. Before the point, the value of K_c is larger, the θ_L decreases faster and the fluctuation is larger, while after the point, the θ_L changes slowly and the fluctuation is smaller. Compared with Fig 4, the θ_L obtained by this method changes more smoothly during switching, which is conducive to reducing the fluctuation of the switching process.

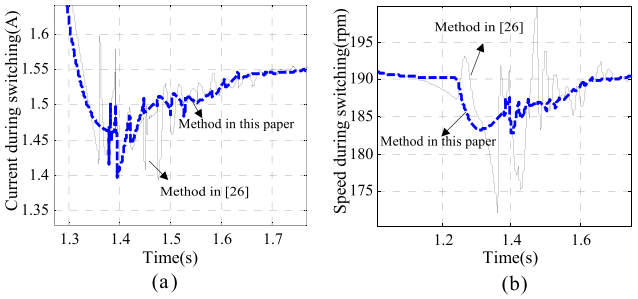

FIGURE 6. Sectionalized and fixed slope switching time i_d and speed waveform:(a) Current fluctuation during the switching process (b) Speed fluctuation during the switching process.

At this point, θ_L is the angle of the estimated rotor d-q reference frame lagging the d*-q* reference frame.

During a given q-axis current reduction, the electromagnetic torque $T_e(t)$ of the motor is:

$$T_e(t) = 1.5p\left(\psi_f + \Delta L i_d\right)\left(i_{q0}^* - K_c \cdot \theta_L^2\right)\cos\left(\theta_L(t)\right) \tag{7}$$

where $\Delta L = L_d$-L_q, (L_d, L_q are the d-axis, q-axis inductances), and ψ_f is the permanent magnet flux linkage. Because the electromagnetic torque is equal to the load torque during this process, the angular error is expressed according to the variation law of the current:

$$\theta_L(t) = \arccos\frac{T_e(t)}{1.5p(\psi_f + \Delta L i_d)\left(i_{q0}^* - K_c \cdot \theta_L^2\right)} \tag{8}$$

$\theta_L(t)$ keeps decreasing following i_q^*(t) according to (8). At the end of the switching process, i_q^* is already equal to i_q, but θ_L has not reached 0° yet due to the slow mechanical response. If the back EMF algorithm is switched, the value of i_q^* will be smaller than the current value matched by the load, which will eventually, lead to the apparent fluctuation of the speed. To ensure the smooth switching of the algorithm, this paper sets the switching when $\theta_L = 5°$.

To verify the effectiveness of the proposed algorithm, experimental verification was carried out in MATLAB/Simulink. The experimental results are shown in Fig. 6. The two algorithms switching at similar times. Compared with the algorithm proposed in [25], fluctuations of speed and the q-axis current are significantly smaller, which controlled by the strategy proposed in this paper.

III. IMPROVED BACK EMF INTEGRATION ALGORITHM

In this paper, the I/f control algorithm is used to start the motor. When the speed reaches steady-state position which is the requirement of the back EMF algorithm, then the value of i_q^* should be reduced. When the difference between the estimated rotor angle and the angle generated by the angle generator is less than a specific range, the I/f control is switched to the back EMF method. However, compared with SPMSM, the mathematical model of IPMSM is complex, and the rotor position information is difficult to extract from back EMF. Therefore, the mathematical model of IPMSM is

analyzed and rewritten to get rotor position. At the same time, the influence of initial value and current sampling error on the accuracy of flux estimation is eliminated, which improves the performance of the algorithm.

A. REWRITING OF THE IPMSM MATHEMATICAL MODEL

The voltage equation of a PMSM in α-β reference frame can be expressed as

$$\mathbf{u_s} = R\mathbf{i_s} + \mathrm{p}\boldsymbol{\psi}_\mathbf{s} \tag{9}$$

where R, p, $\mathbf{u_s}$, $\mathbf{i_s}$ and $\psi_\mathbf{s}$ are the stator resistance, differential operator, voltage vector, current vector and flux linkage vector of the motor in the α-β axis component, respectively.

For ease of analysis, the flux linkage can be expressed in the d-q reference frame as:

$$\boldsymbol{\psi}_\mathrm{s} = \left(\psi_\mathrm{d} + j\psi_\mathrm{q}\right) \cdot \mathrm{e}^{\mathrm{j}\theta_\mathrm{e}} = (L_\mathrm{d} i_\mathrm{d} + \psi_\mathrm{f} + jL_\mathrm{q} i_\mathrm{q})\mathrm{e}^{\mathrm{j}\theta_\mathrm{e}} \tag{10}$$

where ψ_f, ψ_d, ψ_q, L_d, L_q, and $\mathrm{e}^{\mathrm{j}\theta_\mathrm{e}}$ are flux linkage of the rotor permanent magnet, flux linkage vector of d-q reference frame, inductance of the d-q reference frame and the inverse park transformation matrix.

For the position estimation of the rotor, the term $L_\mathrm{q} i_\mathrm{d}$ can be extracted from the above equation (10) and write down as:

$$\begin{aligned}\boldsymbol{\psi}_\mathrm{s} &= \left(\psi_\mathrm{d} + j\psi_\mathrm{q}\right) \cdot \mathrm{e}^{\mathrm{j}\theta_\mathrm{e}} = (L_\mathrm{d} i_\mathrm{d} + \psi_\mathrm{f} + jL_\mathrm{q} i_\mathrm{q})\mathrm{e}^{\mathrm{j}\theta_\mathrm{e}} \\ &= (L_\mathrm{d} i_\mathrm{d} + \psi_\mathrm{f} - L_\mathrm{q} i_\mathrm{d}) \cdot \mathrm{e}^{\mathrm{j}\theta_\mathrm{e}} + (L_\mathrm{q} i_\mathrm{d} + jL_\mathrm{q} i_\mathrm{q})\mathrm{e}^{\mathrm{j}\theta_\mathrm{e}} \\ &= (L_\mathrm{d} i_\mathrm{d} + \psi_\mathrm{f} - L_\mathrm{q} i_\mathrm{d}) \cdot \mathrm{e}^{\mathrm{j}\theta_\mathrm{e}} + L_\mathrm{q} \cdot (i_\alpha + j i_\beta)\end{aligned} \tag{11}$$

Let $L_\mathrm{d} i_\mathrm{d} + \psi_\mathrm{f}$- $L_\mathrm{q} i_\mathrm{d} = \mathrm{A}$ then eq. (11) can be expressed as:

$$\psi_\alpha - L_\mathrm{q} i_\alpha + j(\psi_\beta - L_\mathrm{q} i_\beta) = A(\cos\theta_e + j\sin\theta_e) \tag{12}$$

where θ_e in the equation (11) is the electrical angle of the motor, so the rotor position estimation a formula can be derived as:

$$\theta_\mathrm{e} = \arctan\frac{\psi_\beta - L_\mathrm{q} i_\beta}{\psi_\alpha - L_\mathrm{q} i_\alpha} \tag{13}$$

It can be observed from equations (11) to (13) that above method deduces a new rotor position estimation formula by rewriting the mathematical model of the motor. This method is easy to implement. However, if the flux is directly obtained by integral operation, the calculated result will be affected by the initial value of current and produce DC offset. Moreover, the sampling current itself often contains some DC, which will lead to the zero drift of the estimated flux-linkage. Therefore, this paper will use LPF with the compensation operation and zero drift correction to calculate flux instead of the integral operation.

B. IMPROVED FLUX LINKAGE ESTIMATION ALGORITHM

At steady state, the back EMF phasor $\dot{E}_\alpha$, $\dot{E}_\beta$ and flux linkage phasor $\dot{\psi}_\alpha$, $\dot{\psi}_\beta$ can be expressed as:

$$\begin{cases}\dot{\psi}_\alpha = \dot{E}_\alpha / \mathrm{j}\omega_\mathrm{e} \\ \dot{\psi}_\beta = \dot{E}_\beta / \mathrm{j}\omega_\mathrm{e}\end{cases} \tag{14}$$

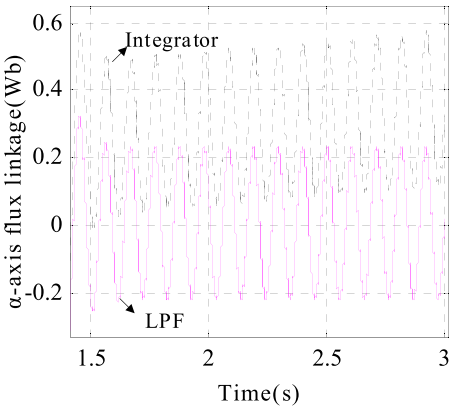

FIGURE 7. Comparison of integrator and LPF.

Replacing the integrator with LPF [35]. And the obtained flux linkage phasor $\dot{\psi}_{\alpha\_\mathrm{lpf}}$, $\dot{\psi}_{\beta\_\mathrm{lpf}}$ by non-gain LPF can be expressed as:

$$\begin{cases}\dot{\psi}_{\alpha\_\mathrm{lpf}} = \dot{E}_\alpha / (\mathrm{j}\omega_\mathrm{e} + \omega_\mathrm{c}) \\ \dot{\psi}_{\beta\_\mathrm{lpf}} = \dot{E}_\beta / (\mathrm{j}\omega_\mathrm{e} + \omega_\mathrm{c})\end{cases} \tag{15}$$

where ω_c represents the cutoff frequency of the LPF.

As shown in Fig. 7, a DC offset of 0.5A is added to i_α and i_β. When the integrator is used, the phenomenon of zero drift and offset will appear. By using LPF, the estimated flux doesn't include zero drift. At the same time, since the numerator of the LPF using in this paper is 1, it also has an inhibitory effect on the DC offset.

Available from equations (14) and (15):

$$\begin{cases}\dot{\psi}_\alpha / \dot{\psi}_{\alpha\_\mathrm{lpf}} = (\mathrm{j}\omega_\mathrm{e} + \omega_\mathrm{c})/\mathrm{j}\omega_\mathrm{e} \\ \dot{\psi}_\beta / \dot{\psi}_{\beta\_\mathrm{lpf}} = (\mathrm{j}\omega_\mathrm{e} + \omega_\mathrm{c})/\mathrm{j}\omega_\mathrm{e}\end{cases} \tag{16}$$

The relationship between $\dot{\psi}_{\alpha\_\mathrm{lpf}}$, $\dot{\psi}_{\beta\_\mathrm{lpf}}$ and $\dot{\psi}_\alpha$, $\dot{\psi}_\beta$:

$$\begin{cases}\dot{\psi}_\alpha = \dot{\psi}_{\alpha\_\mathrm{lpf}} + \dot{\psi}_{\alpha\_\mathrm{lpf}} \cdot \dfrac{\omega_\mathrm{c}}{\mathrm{j}\omega_\mathrm{e}} \\ \dot{\psi}_\beta = \dot{\psi}_{\beta\_\mathrm{lpf}} + \dot{\psi}_{\beta\_\mathrm{lpf}} \cdot \dfrac{\omega_\mathrm{c}}{\mathrm{j}\omega_\mathrm{e}}\end{cases} \tag{17}$$

From equation (16), it can be concluded that at low speed, ω_e is close to the cutoff frequency ω_c of the LPF, and the phase of the estimated value of flux linkage leads the actual value. $\dot{\psi}_{\alpha_\mathrm{lpf}}$and $\dot{\psi}_{\beta\_\mathrm{lpf}}$ must be compensated to get $\dot{\psi}_\alpha$and$\dot{\psi}_\beta$. According to equations (14) and (17), the compensation a formula can be written as:

$$\begin{cases}\dot{\psi}_\alpha = \dot{\psi}_{\alpha\_\mathrm{lpf}} + \dot{\psi}_{\beta\_\mathrm{lpf}} \cdot \dfrac{\omega_\mathrm{c}}{\omega_\mathrm{e}} \\ \dot{\psi}_\beta = \dot{\psi}_{\beta\_\mathrm{lpf}} - \dot{\psi}_{\alpha\_\mathrm{lpf}} \cdot \dfrac{\omega_\mathrm{c}}{\omega_\mathrm{e}}\end{cases} \tag{18}$$

The experimental results are shown in Fig. 8(a). When the motor speed is low, the compensation algorithm can solve the problem that the phase of the LPF estimation value is advanced.

It can be analyzed from Equation (15) that the DC amount in the flux linkage signal is related to the cutoff frequency ω_c.

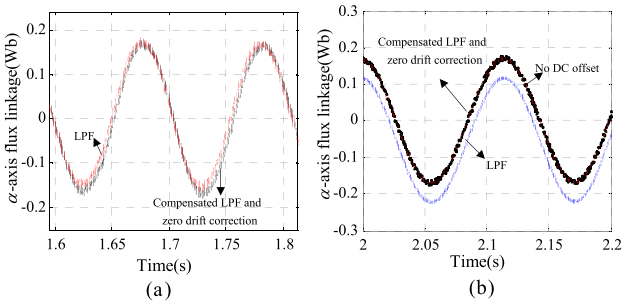

FIGURE 8. Diagram of the experimental results of the α-axis flux linkage: (a) The comparison between the LPF with compensation and simple LPF (b) The experimental results of LPF with the compensation operation and zero drift correction algorithm when i_α has DC offset.

The larger the cutoff frequency ω_c is, the stronger the ability to suppress the offset. However, the LPF can only reduce the DC amount and cannot be eliminated completely. To eliminate the amount of DC, a zero-drift correction method must be used.

To eliminate the DC amount, it is necessary to calculate the amount of DC offset in the flux linkage:

$$\begin{cases} \psi_{\text{dir}\_\alpha} = \dfrac{1}{2}\left(\psi_{\max\_\alpha} - \psi_{\min\_\alpha}\right) \\ \psi_{\text{dir}\_\beta} = \dfrac{1}{2}\left(\psi_{\max\_\beta} - \psi_{\min\_\beta}\right) \end{cases} \tag{19}$$

where $\dot{\psi}_{\max\_\alpha}$ and $\dot{\psi}_{\max\_\beta}$ are the maximum value of the flux linkage in one cycle, $\dot{\psi}_{\min\_\alpha}$ and $\dot{\psi}_{\min\_\beta}$ are the minimum value of the flux linkage, $\dot{\psi}_{\text{dir}\_\alpha}$ and $\dot{\psi}_{\text{dir}\_\beta}$ are the DC offset.

The above zero drift correction algorithm refreshes once every cycle and the algorithm cannot be corrected in real-time. In this paper, the LPF can avoid the zero-drift but cannot eliminate the DC offset. And its inhibitory capacity is related to ω_c. However, the extreme value method can remove the DC offset. So, this method combined the LPF with extreme elimination which can avoid the zero-drift and eliminate the fixed DC offset completely. The experimental results prove this scheme. As shown in Fig. 8(b), the red curve is the flux calculation result when i_α has no DC offset. Black and blue curves are flux calculation results when there is DC offset in i_α. The black curve is obtained by using a LPF and zero-drift correction algorithm proposed in this paper. Moreover, the blue curve just used the LPF algorithm. The black and red curves are coincident. Due to the proposed algorithm, we can effectively eliminate the DC offset and improve estimation accuracy.

IV. EXPERIMENTAL RESULT

As shown in Fig. 9, an experimental platform is built to verify the reliability of the proposed algorithm. This platform mainly includes an IPMSM whose parameters are shown in Table 1, the inverter which uses DSP28335 as a processor, a three-phase asynchronous motor which is used for providing load-torque and other measuring equipment. Meanwhile, a propeller load simulative platform is built by connecting Siemens S120 inverter with MATLAB software.

FIGURE 9. Schematic diagram of the experimental platform.

TABLE 1. Parameters of PMSM.

Symbol	Description	Value
P	Rated power	2.2 KW
i_N	Rated Current	4 A
n	Rated speed	750 rpm
R	Stator resistance	6 Ω
p	Number of pole-pairs	3 pairs
L_d	d-axis inductance	43.5 mH
L_q	q-axis inductance	133.3 mH
ψ	Rotor flux linkage	0.169 Wb
J	Inertia	3.708×10^{-3} kg.m^2

This platform simulates the characteristics of the ship propeller load. The control algorithm proposed in this paper will be tested on this experimental platform.

The overall process of the control strategy designed in this paper is:

1. The motor rotor pre-positioning process by injecting DC twice.

2. Constant current acceleration process. In this process, the current is set to a fixed value of 4A. After 2s, the speed reaches a stable speed.

3. I/f control and back EMF algorithm switching process is designed to control stator current control strategy of reduce motor q-axis current, when θ_L is less than 5°, the system switches to back EMF control algorithm

4. An improved back EMF algorithm is used to eliminate the DC offset and to improve the estimation performance of the algorithm.

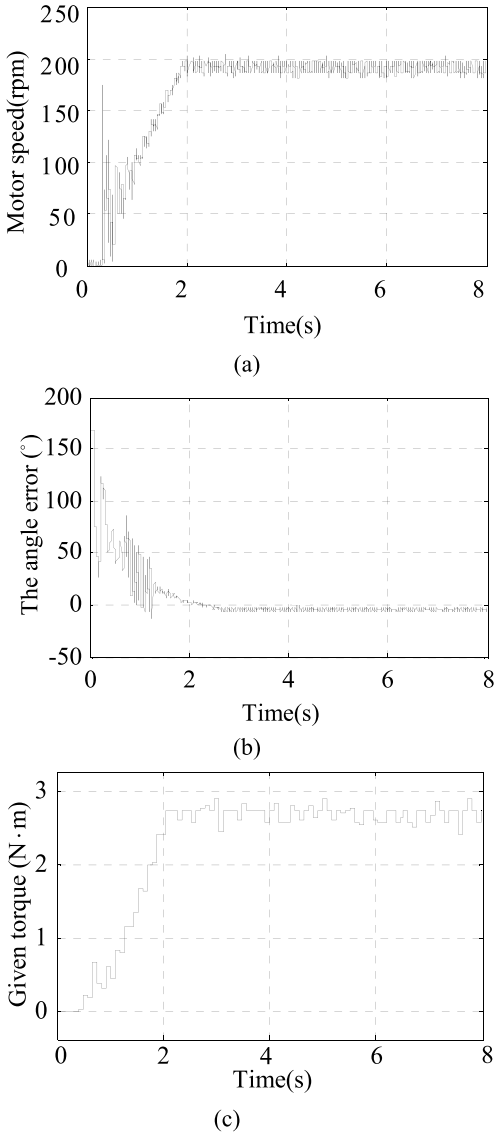

FIGURE 10. Experimental results of open-loop initiation: (a) Rotor speed during startup. (b) Setup behavior of angle which is the angle err between the estimated rotor q-axis based on the improved back EMF and the real rotor q-axis measured by the encoder. (c) Load motor given torque.

In this experiment, when the motor speed reaches 190rpm, then the motor will adopt the back EMF algorithm, and the load connected to the motor is the propeller load. Moreover, rotor pre-positioning of the motor at 0s and at 0.2s, we used I/f control strategy to start the motor. The motor achieved the steady speed at 2s. The given q-axis current i_q^* is started to decrease at 2.2s. When θ_L is less than 5°, then I/f control is switched to the back EMF algorithm.

A. OPEN-LOOP STARTUP PROCESS

Fig.10 represents the operation result during the motor startup. Time from 0-0.2s is the process of pre-positioning, and 0.2-2s is the process of motor speed establishment. In this process, the motor speed fluctuates greatly. However, after the adjustment time of about 0.4s, the motor speed

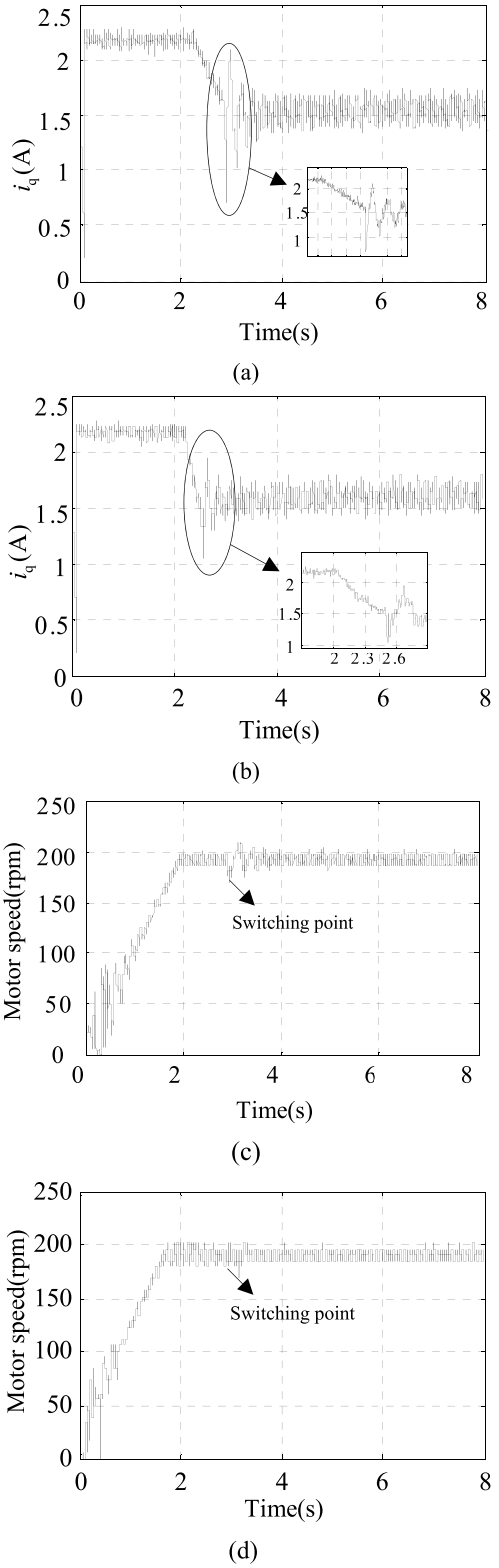

FIGURE 11. Experimental results during switching: (a) The experimental result of i_q, which is obtained by reducing the q-axis current with the method proposed in [26] (b) The experimental result of i_q, which is obtained by the method proposed in this paper, (c) The experimental result of motor speed, which is obtained by reducing the q-axis current with the method proposed in [26] (d) The experimental result of motor speed, which is obtained by the method proposed in this paper.

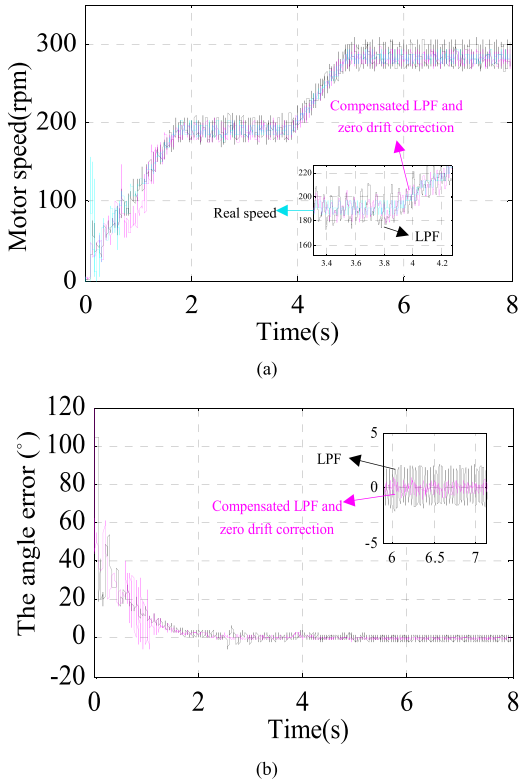

FIGURE 12. Dynamic performance test of improved back EMF integration algorithm: (a) Experimental comparison of the actual speed and the speed of improved estimation algorithm (b) Setup behavior of angle θ_L under different algorithms, which is the error angle between the estimated rotor q-axis position based on the improved back EMF and the real rotor q-axis position measured by the encoder.

can steadily follow the given speed and finally stabilize at 190rpm. In the beginning, the error of the estimated angle is relatively large. When the speed is stable, the rotation can be seen from Fig.10 (b) that since no closed loop is used here, there is always a steady-state error and the estimated angle is consistent with the actual angle which conforms to the conditions of algorithm switching. Meanwhile, the propeller load simulation system calculates the torque of the actual load motor according to the real-time speed. The torque output value is shown in Fig. 10 (c). It is related to the speed and it confirms to the load characteristics of propeller [30].

B. CONTROL STRATEGY SWITCHING PROCESS

Fig. 11 represents the current and speed test result during the switching process. The smooth switch process occurs after around 2.5s from the experimental results. By comparing Fig. 11(a) and (b), it can be clearly seen that the proposed algorithm effectively reduces the fluctuation of the q-axis current of the motor. As shown in Fig. 11(a) and (b), the motors speed has almost no fluctuation during the algorithm switching process, which much guarantees the stability of the motor running. Compared with the control algorithm in [25], the current fluctuation and the speed fluctuation can be significantly reduced.

C. EXPERIMENT TO VERIFY THE RELIABILITY OF ALGORITHM

Fig. 12(a) shows the comparison between actual rotational speed measured by the encoder, rotational speed estimated by the method without zero-drift correction and method proposed in this paper. Estimated rotational speed using the LPF with zero-drift correction is the closest to the encoder measured rotational speed. It can be seen from Fig. 12(b) that the angular error of the estimated rotational speed and encoder rotational speed using the zero-drift correction is smaller and more stable during the operation. Finally, a speed ramp is set to test the following performance of the estimation algorithm. It can be seen from the Fig.12(c) that the estimated speed is always consistent with the measured speed of the encoder and a small deviation and excellent dynamic performance.

V. CONCLUSION

I/f control combined with back EMF scheme is a practical and reliable sensorless control strategy for driving ship propeller. Relying on I/f control, the motor can start from zero speed to stable speed with propeller load even if there is no encoder feedback rotor position information at low speed. In the process of switching, a new current control method is proposed to reduce the speed and current ripple. According to the relationship between θ_L and i_q^*, the change curve of θ_L can be automatically controlled by using this method and then a stable switching point can be selected for switching, and to ensure the smooth operation of the motor. To ensure the accuracy of θ_L and the precise control of the motor, the exact rotor position needs to be obtained when the motor is running at medium and high speed. A simple flux estimation method is adopted for IPMSM in this paper. The phase delay of flux estimated by LPF is modified by compensation and the bias of current sampling is calculated by the extremum method. Detailed analysis and design guides for the current regulation startup strategy and flux improved estimated method are also given and are validated using simulation and experimental results.

REFERENCES

[1] Y. Dai, L. Song, and S. Cui, "Development of PMSM drives for hybrid electric car applications," *IEEE Trans. Magn.*, vol. 43, no. 1, pp. 434–437, Jan. 2007.

[2] D. Li, T. Suzuki, K. Sakamoto, Y. Notohara, T. Endo, C. Tanaka, and T. Ando, "Sensorless control and PMSM drive system for compressor applications," in *Proc. CES/IEEE 5th Int. Power Electron. Motion Control Conf.*, Aug. 2006, pp. 1–5.

[3] H. Lin, H. Guo, and H. Qian, "Design of high-performance permanent magnet synchronous motor for electric aircraft propulsion," in *Proc. 21st Int. Conf. Electr. Mach. Syst. (ICEMS)*, 2018, pp. 174–179.

[4] M. Hasoun, A. E. Afia, K. Chikh, M. Khafallah, and K. Benkirane, "A PWM strategy for dual three-phase PMSM using 12-sector vector space decomposition for electric ship propulsion," in *Proc. 19th IEEE Medit. Electrotech. Conf. (MELECON)*, May 2018, pp. 243–248.

[5] J. F. Hansen and F. Wendt, "History and state of the art in commercial electric ship propulsion, integrated power systems, and future trends," *Proc. IEEE*, vol. 103, no. 12, pp. 2229–2242, Dec. 2015.

[6] E. Bostanci, M. Moallem, A. Parsapour, and B. Fahimi, "Opportunities and challenges of switched reluctance motor drives for electric propulsion: A comparative study," *IEEE Trans. Transport. Electrific.*, vol. 3, no. 1, pp. 58–75, Mar. 2017.
[7] J. M. Apsley, A. Gonzalez-Villasenor, M. Barnes, A. C. Smith, S. Williamson, J. D. Schuddebeurs, P. J. Norman, C. D. Booth, G. M. Burt, and J. R. McDonald, "Propulsion drive models for full electric marine propulsion systems," *IEEE Trans. Ind. Appl.*, vol. 45, no. 2, pp. 676–684, Mar. 2009.
[8] G. Patterson, T. Koseki, Y. Aoyama, and K. Sako, "Simple modeling and prototype experiments for a new high-thrust low-speed permanent-magnet disk motor," *IEEE Trans. Ind. Appl.*, vol. 47, no. 1, pp. 65–71, Jan./Feb. 2011.
[9] S.-Y. Kim, Y.-D. Yoon, and S.-K. Sul, "Suppression of thrust loss for the maximum thrust operation in the electric propulsion ship," *IEEE Trans. Ind. Appl.*, vol. 45, no. 2, pp. 756–762, Mar./Apr. 2009.
[10] T. D. Batzel and K. Y. Lee, "Electric propulsion with the sensorless permanent magnet synchronous motor: Model and approach," *IEEE Trans. Energy Convers.*, vol. 20, no. 4, pp. 818–825, Dec. 2005.
[11] M. Linke, R. Kennel, and J. Holtz, "Sensorless position control of permanent magnet synchronous machines without limitation at zero speed," in *Proc. IEEE 28th Annu. Conf. Ind. Electron. Soc. (IECON)*, Nov. 2002, pp. 674–679.
[12] P. L. Jansen and R. D. Lorenz, "Transducerless position and velocity estimation in induction and salient AC machines," *IEEE Trans. Ind. Appl.*, vol. 31, no. 2, pp. 240–247, Mar. 1995.
[13] S.-I. Kim, J.-H. Im, E.-Y. Song, and R.-Y. Kim, "A new rotor position estimation method of IPMSM using all-pass filter on high-frequency rotating voltage signal injection," *IEEE Trans. Ind. Electron.*, vol. 63, no. 10, pp. 6499–6509, Oct. 2016.
[14] G. Wang, R. Liu, N. Zhao, D. Ding, and D. Xu, "Enhanced linear ADRC strategy for HF pulse voltage signal injection-based sensorless IPMSM drives," *IEEE Trans. Power Electron.*, vol. 34, no. 1, pp. 514–525, Jan. 2019.
[15] P. L. Xu and Z. Q. Zhu, "Novel square-wave signal injection method using zero-sequence voltage for sensorless control of PMSM drives," *IEEE Trans. Ind. Electron.*, vol. 63, no. 12, pp. 7444–7454, Dec. 2016.
[16] M. Schroedl and R. S. Wieser, "EMF-based rotor flux detection in induction motors using virtual short circuits," *IEEE Trans. Ind. Appl.*, vol. 34, no. 1, pp. 142–147, Jan. 1998.
[17] T.-S. Kwon, M.-H. Shin, and D.-S. Hyun, "Speed sensorless stator flux-oriented control of induction motor in the field weakening region using Luenberger observer," *IEEE Trans. Power Electron.*, vol. 20, no. 4, pp. 864–869, Jul. 2005.
[18] M. Hinkkanen, L. Harnefors, and J. Luomi, "Reduced-order flux observers with stator-resistance adaptation for speed-sensorless induction motor drives," *IEEE Trans. Power Electron.*, vol. 25, no. 5, pp. 1173–1183, May 2010.
[19] N. T. West and R. D. Lorenz, "Digital implementation of stator and rotor flux-linkage observers and a stator-current observer for deadbeat direct torque control of induction machines," *IEEE Trans. Ind. Appl.*, vol. 45, no. 2, pp. 729–736, Mar. 2009.
[20] G. Foo and M. F. Rahman, "Sensorless sliding-mode MTPA control of an IPM synchronous motor drive using a sliding-mode observer and HF signal injection," *IEEE Trans. Ind. Electron.*, vol. 57, no. 4, pp. 1270–1278, Apr. 2010.
[21] L. Fan, T. Yang, M. Rashed, and S. Bozhko, "Sensorless control of dual-three phase PMSM based aircraft electric starter/generator system using model reference adaptive system method," in *Proc. CSAA/IET Int. Conf. Aircr. Utility Syst. (AUS)*, 2018, pp. 787–794.
[22] P. D. C. Perera, F. Blaabjerg, J. K. Pedersen, and P. Thogersen, "A sensorless, stable V/f control method for permanent-magnet synchronous motor drives," *IEEE Trans. Ind. Appl.*, vol. 39, no. 3, pp. 783–791, May 2003.
[23] C. L. Baratieri and H. Pinheiro, "An I-F starting method for smooth and fast transition to sensorless control of BLDC motors," in *Proc. Brazilian Power Electron. Conf.*, 2013, pp. 836–843.
[24] M. Fatu, R. Teodorescu, I. Boldea, G. Andreescu and F. Blaabjerg, "I-F starting method with smooth transition to EMF based motion-sensorless vector control of PM synchronous motor/generator," in *Proc. IEEE Power Electron. Spec. Conf.*, Rhodes, 2008, pp. 1481–1487.
[25] C. Wang and L. Xu, "A novel approach for sensorless control of PM machines down to zero speed without signal injection or special PWM technique," *IEEE Trans. Power Electron.*, vol. 19, no. 6, pp. 1601–1607, Nov. 2004.
[26] Z. Wang, K. Lu, and F. Blaabjerg, "A simple startup strategy based on current regulation for back-EMF-based sensorless control of PMSM," *IEEE Trans. Power Electron.*, vol. 27, no. 8, pp. 3817–3825, Aug. 2012.
[27] R. Wu and G. R. Slemon, "A permanent magnet motor drive without a shaft sensor," *IEEE Trans. Ind. Appl.*, vol. 27, no. 5, pp. 1005–1011, Sep. 1991.
[28] R. Ortega, L. Praly, A. Astolfi, J. Lee, and K. Nam, "Estimation of rotor position and speed of permanent magnet synchronous motors with guaranteed stability," *IEEE Trans. Control Syst. Technol.*, vol. 19, no. 3, pp. 601–614, May 2011.
[29] Y. Wang and R. D. Lorenz, "Using volt-sec. Sensing to extend the low speed range and the disturbance rejection capability of back-EMF-based self-sensing," in *Proc. 18th Eur. Conf. Power Electron. Appl. (EPE ECCE Eur.)*, 2016, pp. 1–10.
[30] I. Boldea, M. C. Paicu, and G. D. Andreescu, "Active flux concept for motion-sensorless unified AC drives," *IEEE Trans. Power Electron.*, vol. 23, no. 5, pp. 2612–2618, Sep. 2008.
[31] K. Lu, X. Lei, and F. Blaabjerg, "Artificial inductance concept to compensate nonlinear inductance effects in the back EMF-based sensorless control method for PMSM," *IEEE Trans. Energy Convers.*, vol. 28, no. 3, pp. 593–600, Sep. 2013.
[32] F. Meng, C. Zhang, and Y. Zhao, "Modeling and simulation of marine propeller load," in *Proc. IEEE Int. Conf. Mechtron. Automat.*, Aug. 2016, pp. 2371–2375.
[33] J. Ren, H. Feng, H. Ren, and Y. Huang, "Simulation of PMSM vector control system based on propeller load characteristic," in *Proc. Int. Conf. Intell. Control Inf. Process.*, 2010, pp. 735–737.
[34] P. Balazovic and R. Filka, "Sensorless PMSM control for H-axis washing machine drive," in *Proc. IEEE Power Electron. Spec. Conf.*, Rhodes, 2008, pp. 4237–4242.
[35] S. Koonlaboon and S. Sangwongwanich, "Sensorless control of interior permanent-magnet synchronous motors based on a fictitious permanent-magnet flux model," in *Proc. 40th IAS Annu. Meeting Conf. Rec. Ind. Appl. Conf.*, 2005, pp. 311–318.

ZHENRUI ZHANG was born in Shandong, China, in 1994. He received the B.E. degree in marine engineering from Yantai University, Yantai, China, in 2017. He is currently pursuing the Ph.D. degree in marine engineering with Dalian Maritime University, Dalian, China. His research interest includes sensor-less control technology for ac motor.

HAOHAO GUO was born in Jiangxi, China, in 1984. He received the B.Eng. and M.Eng. degrees in marine engineering from Dalian Maritime University, Dalian, China, in 2007 and 2012, respectively. He is currently working as a Lecturer with the Marine Engineering College, Dalian Maritime University. His current research interest includes control of marine permanent magnet propulsion motor.

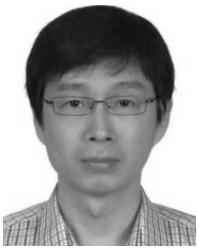

YANCHENG LIU received the B.Eng. and M.Eng. degrees in electrical engineering from the Harbin Institute of Technology, Harbin, China, in 1985 and 1988, respectively, and the Ph.D. degree in marine engineering from Dalian Maritime University, Dalian, China, in 2002. He is currently a Professor with the Marine Engineering College, DMU. His current research interests include electric drive and control and electric marine vehicles.

QIAOFEN ZHANG was born in Fujian, China, in 1986. She received the B.Eng. degree in electrical engineering and automation, the M.Eng. degree in power system and automation, and the Ph.D. degree in marine engineering from Dalian Maritime University, Dalian, China, in 2009, 2011, and 2016, respectively.

From 2017 to 2018, she worked as a Teacher with the Electronic Engineering Department of Dalian Neusoft Institute of Information. She is currently a Researcher in the postdoctoral station of control science and engineering station with Dalian Maritime University. Her current research interest includes control of marine permanent magnet propulsion motor.

PENGLI ZHU received the B.Eng. degree in marine engineering from Dalian Maritime University (DMU), Dalian, China, in 2017, where he is currently pursuing the M.Eng. degree. His current research interests include pattern recognition and autonomous navigation of unmanned underwater vehicles.

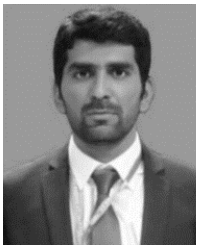

RASHID IQBAL was born in Pakistan. He received the M.S.E.E. degree in electrical engineering from Bahira University, Islamabad, Pakistan, in 2017. He is currently pursuing the Ph.D. degree with the School of Marine Engineering Collage, Dalian Maritime University, Dalian, China. From 2014 to 2019, he was a Lecturer with Bahira University. He was a Trainee Engineer with Warid Telecom, from 2012 to 2014. His research interests include motor drives, control, and electric marine drives.